AGU PUBLICATIONS

Geophysical Research Letters

RESEARCH LETTER
10.1002/2014GL061606

Key Points:
- A warming trend of NE Pacific middepth waters occurred over the past 43 years
- This seawater warming caused Cascadia margin methane hydrates to dissociate
- The volume of released methane is quantified and projected through 2100

Supporting Information:
- Readme
- Text S1
- Figure S1
- Figure S2
- Figure S3
- Figure S4
- Figure S5

Correspondence to:
S. L. Hautala and E. A. Solomon,
hautala@u.washington.edu;
esolomn@u.washington.edu

Citation:
Hautala, S. L., E. A. Solomon, H. P. Johnson, R. N. Harris, and U. K. Miller (2014), Dissociation of Cascadia margin gas hydrates in response to contemporary ocean warming, *Geophys. Res. Lett.*, *41*, 8486–8494, doi:10.1002/2014GL061606.

Received 19 AUG 2014
Accepted 31 OCT 2014
Accepted article online 4 NOV 2014
Published online 5 DEC 2014

Dissociation of Cascadia margin gas hydrates in response to contemporary ocean warming

Susan L. Hautala[1], Evan A. Solomon[1], H. Paul Johnson[1], Robert N. Harris[2], and Una K. Miller[1]

[1]School of Oceanography, University of Washington, Seattle, Washington, USA, [2]College of Earth, Ocean, and Atmospheric Sciences, Oregon State University, Corvallis, Oregon, USA

Abstract Gas hydrates, pervasive in continental margin sediments, are expected to release methane in response to ocean warming, but the geographic range of dissociation and subsequent flux of methane to the ocean are not well constrained. Sediment column thermal models based on observed water column warming trends offshore Washington (USA) show that a substantial volume of gas hydrate along the entire Cascadia upper continental slope is vulnerable to modern climate change. Dissociation along the Washington sector of the Cascadia margin alone has the potential to release 45–80 Tg of methane by 2100. These results highlight the importance of lower latitude warming to global gas hydrate dynamics and suggest that contemporary warming and downslope retreat of the gas hydrate reservoir occur along a larger fraction of continental margins worldwide than previously recognized.

1. Introduction

Gas hydrates represent one of the largest reservoirs of organic carbon on Earth [*Boswell and Collett*, 2011]. As the upper limit of gas hydrate stability deepens in response to ocean warming, the additional flux of hydrate-derived methane could contribute to ocean acidification, oxygen consumption in the water column, and upper continental slope instability, as well as potentially increased emissions of CH_4 and methane-derived CO_2 to the atmosphere [e.g., *Revelle*, 1983]. Recent studies of gas hydrate dynamics associated with contemporary warming have focused on the Arctic [*Berndt et al.*, 2014; *Westbrook et al.*, 2009; *Thatcher et al.*, 2013; *Reagan et al.*, 2011; *Biastoch et al.*, 2011], with less attention given to the vulnerability of the much larger methane reservoir present at lower latitudes.

Gas hydrates are stable under conditions of low temperature and high pressure, and they typically exist within the top few hundred meters of continental slope sediments. The depth where the gas hydrate stability field pinches out and vanishes (typically along the upper continental slope; termed the feather edge of gas hydrate stability) is dependent on bottom water temperature and local geothermal gradients and represents one of the most climate-sensitive boundaries in the global gas hydrate reservoir [*Boswell and Collett*, 2011; *Ruppel*, 2011]. Upper continental slope gas hydrates are more sensitive to warming than other deposits because of their proximity to transient seawater temperatures at the seafloor, allowing dissociation on relatively short time scales—a few decades compared to 10^2 to 10^3 years for other climate-sensitive reservoirs such as those associated with thinning Arctic permafrost [*Berndt et al.*, 2014; *Ruppel*, 2011]. Recent field and modeling studies show that part of the methane released to the Arctic Ocean at the upper continental slope off West Svalbard is due to ongoing gas hydrate dissociation in response to bottom water warming [*Berndt et al.*, 2014; *Westbrook et al.*, 2009; *Thatcher et al.*, 2013; *Reagan et al.*, 2011].

Although lower latitude hydrates represent a large percentage of the global methane inventory, there are few studies on the vulnerability of these systems to warming of water at the seafloor [e.g., *Kennett et al.*, 2003]. A recent study considered the response of the Carolina Rise hydrate system in the North Atlantic to seawater temperature changes caused by a probable Holocene Gulf Stream shift, with implications for continued future warming [*Phrampus and Hornbach*, 2012]. The degree of seafloor ocean warming directly impacting gas hydrate systems will depend on regional currents and water masses. In particular, circulation affecting the eastern Pacific margins is fundamentally different than for the western North Atlantic. The methane hydrate-rich Washington margin has a dense set of archived water column data (Figure 1) that records systematic warming over the last four decades at the depth of upper continental slope gas hydrates. Using a sediment model with an upper boundary condition tightly constrained by these observations, we find that warming of the North Pacific at the depth corresponding to intermediate water is likely to have a

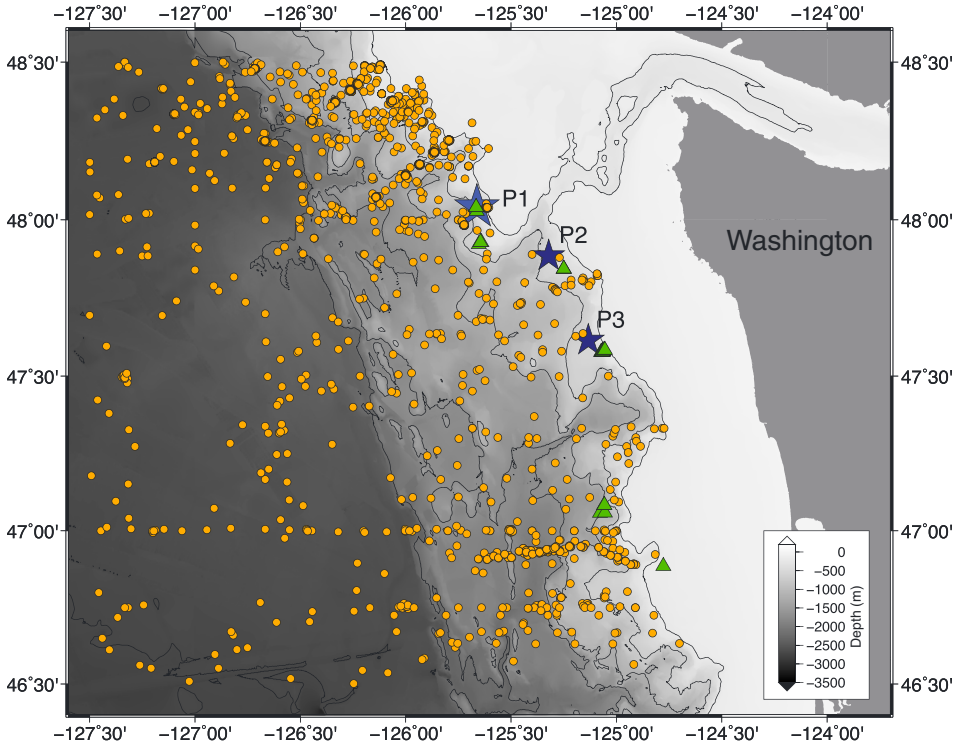

Figure 1. Map of data locations. Bathymetry of the Washington continental slope from GeoMapApp with locations of compiled vertical profiles of conductivity-temperature-depth (CTD) observations shown as orange dots. The locations of bathymetric transects P1–P3 are denoted by blue stars (the length of transects is quite short at the map scale), and the locations of known methane seep sites are denoted by green triangles. The contours for water depth are set at 300 m, 500 m, and then every 500 m.

substantial impact on the Cascadia margin gas hydrate reservoir. This finding has worldwide implications for other upper continental slope reservoirs that are typically bathed in intermediate and lower thermocline waters.

2. Methods

2.1. Water Column Temperature Data

High-resolution conductivity-temperature-depth (CTD), glider, and Argo float temperature profiles extending to a depth of at least 200 m were extracted at observed levels from the World Ocean Database 2013 (National Oceanographic Data Center (NODC)) for the region 124.5°W to 127.5°W and 46.5°N to 48.5°N (Figure 1). Available data span the years 1968 to 2013. We added several CTD casts from an August 2013 field program in the immediate vicinity of methane bubble plume sites to the data from the NODC archive. If only pressure was available in the NODC archive, temperature sampling depth was estimated using the TEOS-10 Gibbs Seawater Oceanographic Toolbox [*McDougall and Barker*, 2011] at the latitude of the profile; otherwise, reported depth values were retained. Entire profiles containing clearly erroneous values, i.e., negative temperatures or temperature values >16°C or <4°C at 200 m, were eliminated, as were profiles taken within the topographically unique Juan de Fuca Canyon. The remaining 2122 open-ocean temperature profiles were linearly interpolated to 10 m depth intervals ranging from 50 to 1000 m. To remove bias from an uneven seasonal sampling distribution (for example, at 480 m depth, monthly average temperature varies over the year by 0.27°C with warmest values in August), long-term monthly average values were subtracted from the data.

To quantitatively estimate the local rate of seawater warming in the presence of sampling biases related to geographical temperature gradients and substantial decadal variability, we performed a multivariate linear regression (Figure 2). In addition to the dependency of interest (sampling year), other independent variables for the multivariate linear regression are latitude, water depth estimated by linearly interpolating

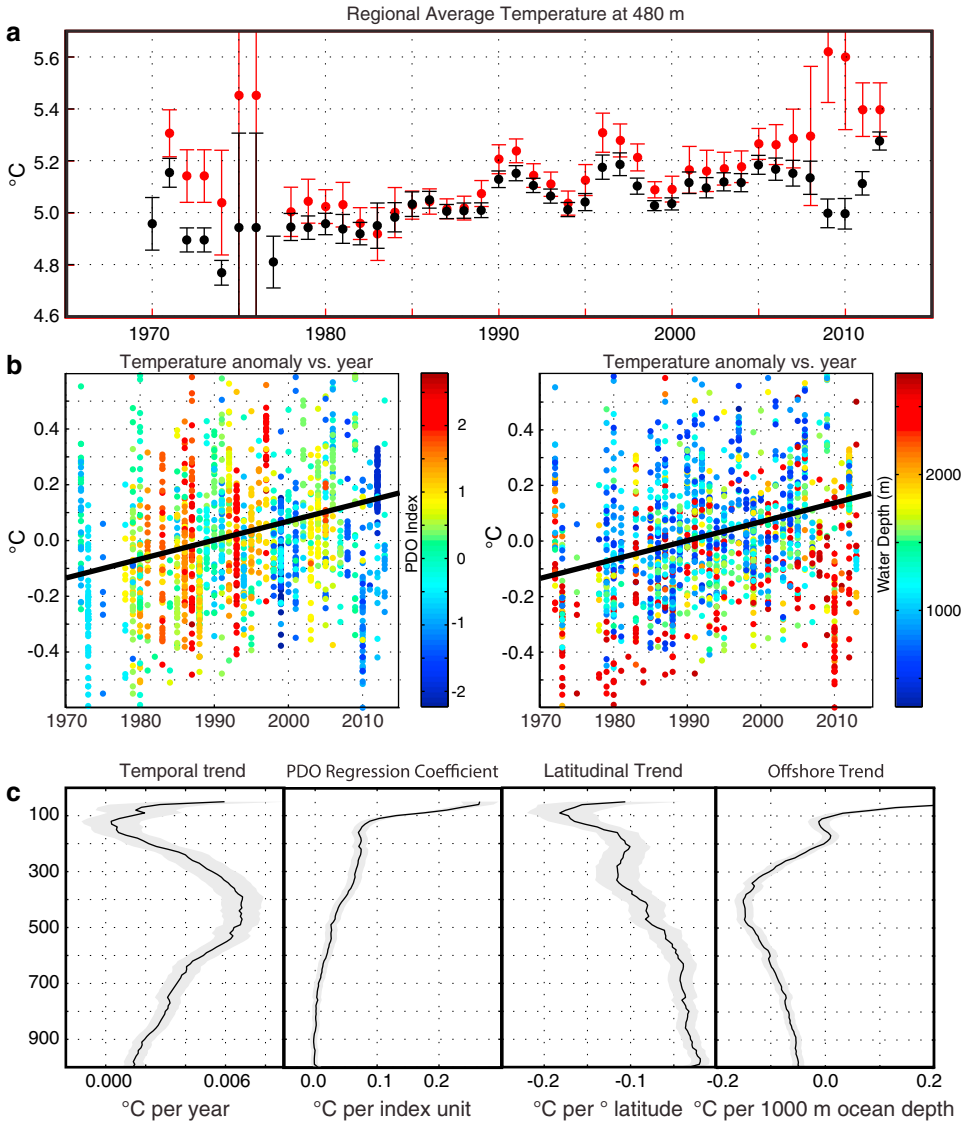

Figure 2. (a) Open-ocean warming record off the Pacific Northwest for water depths greater than 200 m. The black symbols show the 3 year average temperatures, centered on the year shown on the *x* axis, at 480 m for the data shown in Figure 1 with *t* test 95% confidence level error bars. The red symbols show the averages and error bars using only data from water depths between 200 and 1000 m. (b) Raw temperature anomaly, defined by subtracting the long-term regional monthly average value, at 480 m versus year of observation and color coded by PDO index and water depth. The solid line shows the warming trend of 0.0068 ± 0.0009°C yr^{-1}, estimated from a multivariate linear regression (see Methods). The adjusted R^2 at this depth is 0.22. (c) Regression coefficients for each of the four independent variables as a function of depth, with 95% confidence interval error estimates shaded gray.

the 0.5′ SRTM30 PLUS bathymetry data [*Sandwell and Smith*, 2009; *Becker et al*., 2009] at each sampling location, and the monthly Pacific Decadal Oscillation (PDO) index [*Zhang et al*., 1997; *Mantua et al*., 1997] from the Joint Institute for the Study of the Atmosphere and Ocean website at the University of Washington. Unlike Figure 2a, interannual to decadal variability visually dominates the regional average time series in the upper ocean (not shown), and the correlation between temperature and the Pacific Decadal Oscillation (Figure 2c) is large and positive, as expected [*Zhang et al*., 1997; *Mantua et al*., 1997]. The PDO index during the months of our observations ranges from −2.23 to +2.83, with values over +2.0 sampled only between 1983 and 1998 and with negative indices sampled since 2010 (Figure 2b). A sensitivity study (see Table S1 in the supporting information) was conducted to understand how various assumptions impact the regression-derived warming trend at 480 m. Of particular interest are cases where slightly different subsets of

the data are used: data collected only over the slope, data collected only since 1980, adding data within the Juan de Fuca canyon, and excluding Argo and glider data. Sensitivity calculations using different methodological choices yield a warming trend that ranges from +0.0061 to +0.0080°C yr^{-1} and agree within error bars with our best estimate shown in Figures 2b and 2c.

2.2. Sediment Thermal Model

To evaluate the response of the gas hydrate reservoir to the observed warming trend, we first estimate the temperature at the seafloor at a given location and year that is solely associated with long-term climate variation (i.e., under neutral PDO conditions), using the regression coefficients shown in Figure 2 and differences in latitude, water depth, and year from average values for the compiled data (47.9798°N, 1291 m, and 1992, respectively). We focus on three individual bathymetric transects across the Washington margin with differing topography at the up-slope limit of gas hydrate stability (Figure 1). Temperature at the seafloor is estimated from the regression along these transects at the beginning (1970) and end (2013) of the observation period, resulting in a change of +0.29°C at 480 m water depth (Figure 2b).

A 2-D thermal model is used to simulate the change in sediment temperature distribution over this time period (Figure 3) along with the volume of the gas hydrate stability zone, its downslope retreat, and the associated mass of gas hydrate affected by bottom water warming (Figures S1–S4 in the supporting information). This model is based on a finite element heat flow model with prescribed initial and boundary conditions [*Wang et al*., 1995]. Model cells have dimensions of 100 m horizontally and 2 m vertically in the upper 100 m of the sediment column, increasing to 20 m between 100 and 200 m below seafloor (bsf). The base of the model is sufficiently deep to avoid boundary effects, and we prescribe a constant basal heat flux of 60 mW m^{-2} based on nearby heat flow data derived from bottom-simulating reflectors [*Booth-Rea et al*., 2008]. Thermal conductivity and heat capacity are constant throughout the model domain with values of 0.92 W m^{-1} K^{-1} and 2.52×10^6 J km^{-3}. These parameters yield a thermal diffusivity of 3.8×10^{-7} m s^{-2}, consistent with the observed values (see supporting information). At each location along the bathymetric transects, the upper boundary condition for the sediment column is set by the PDO-neutral 1970 temperature estimate. The initial condition is a steady state heat flux matching this upper boundary condition. Transient solutions are calculated with an interval of 1 year. The base of the gas hydrate stability zone is computed assuming Structure I gas hydrate and hydrostatic conditions [*Tishchenko et al*., 2005]. The latent heat of gas hydrate dissociation was not included in our simulations, producing a maximum estimate for the total volume of sediment affected by a vertical shift in the gas hydrate stability zone.

2.3. Projected Seafloor Temperature

Projections of seafloor temperature are based on global average surface air temperature projections from the Intergovernmental Panel on Climate Change (IPCC) Fourth Assessment Report (AR4) report [*Meehl et al*., 2007]. We first extrapolate the observed temperature trend in our data, as determined by the regression analysis, backward in time to 1950. We consider a simple extrapolation of the observed trend forward in time to 2100 to be a conservative scenario, noting that such behavior resembles IPCC emission-stabilized projections and that the local observed trend at 480 m depth (+0.0068°C yr^{-1}) is considerably smaller than the global average air temperature trend over the rest of this century using even the most optimistic (emission-reducing) scenario, Representative Concentration Pathway 2.6 (RCP2.6) in AR5 (+0.0105°C yr^{-1}). The highest emission A1F1 scenario in AR4 shows a global warming of +4.0°C in 2090–2099 relative to 1980–1999, an average warming trend of +0.0381°C yr^{-1}. Note that the highest emission scenario, RCP8.5, in AR5 yields a similar average warming trend of +0.0389°C yr^{-1} [*Stocker et al*., 2013]. Local subsurface water values projected for 2100 are estimated from these global average surface air temperature projections through scaling them by the ratio of the warming trend observed in our data at 480 m to the reported global average AR4 trend in measured air temperature since 1950 (+0.013°C yr^{-1}).

3. Observed Long-Term Warming in the Cascadia Water Column

Water column warming observed in the CTD data shown in Figure 1 is summarized in Figure 2. In Figure 2a, we highlight the regional average record of water column warming at 480 m, corresponding to the up-slope limit of gas hydrate stability in 1970. Latitudinal and offshore temperature gradients determined from the regression analysis (Figure 2c) are consistent with large-scale circulation. Below 200 m, isotherms tilt

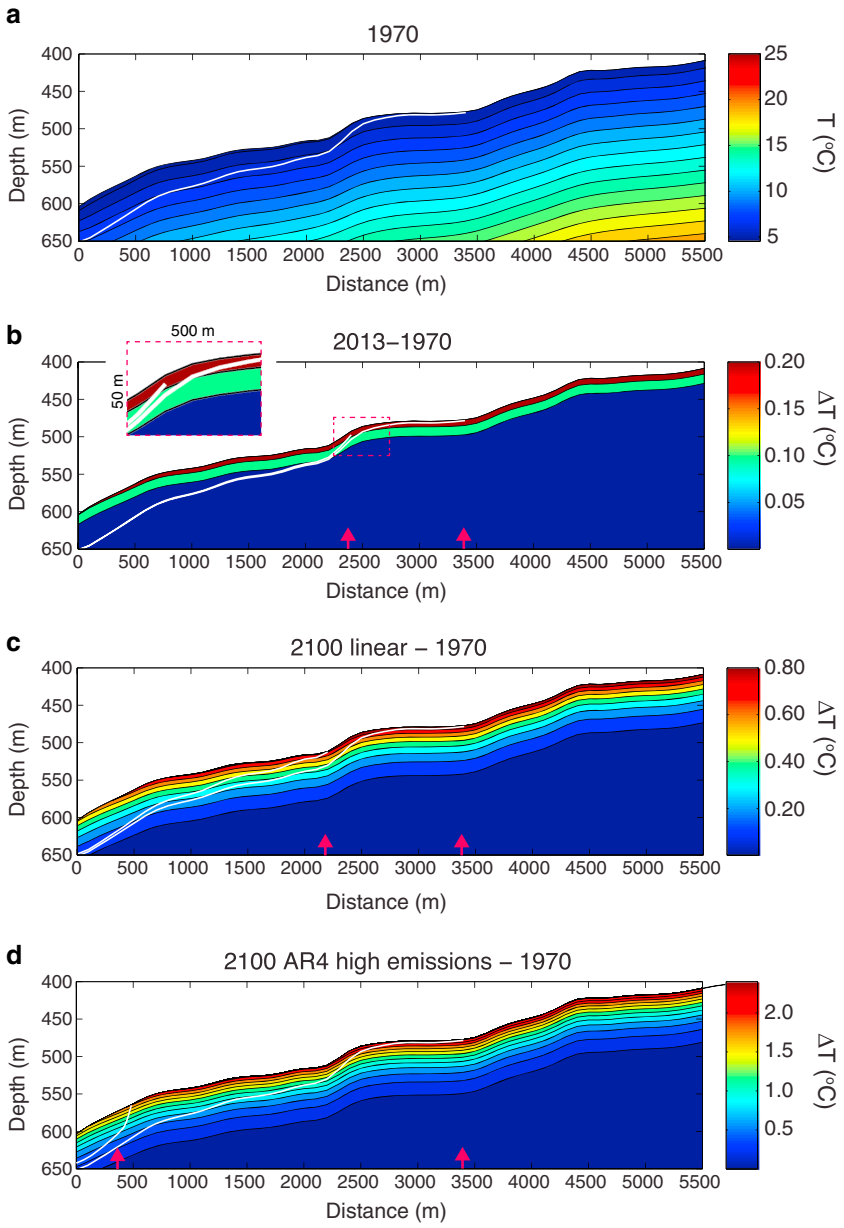

Figure 3. Sediment thermal simulations for bathymetric transect P1. (a) Initial subseafloor temperature distribution in 1970 based on the regression (see Methods) and a basal heat flow of 60 mW/m^2 [*Booth-Rea et al.*, 2008]. The white line is the base of the gas hydrate stability zone (BGHSZ) in the sediment column for Structure I gas hydrate and hydrostatic pressure following the methods outlined in *Tishchenko et al.* [2005]. (b) The simulated change in sediment temperature between 1970 and 2013 and the corresponding shift in the BGHSZ. The BGHSZ shoals over a broad area in response to warming, accompanied by a retreat of its landward edge (indicated by red arrows). (c) Simulated change in sediment temperature between 1970 and 2100 based on the linear extrapolation of seafloor temperature. The upper white line is the BGHSZ in 2100. (d) Simulated change in sediment temperature between 1970 and 2100 based on the high-emission AR4 projection. The upper white line is the BGHSZ in 2100, and the lower white line is the BGHSZ in 1970.

downward approaching the shelf, reflecting some northward flow down to at least 1000 m above the slope [*Hickey*, 1979]. With its core at ~200 m, the California Undercurrent is associated with an intensification of this northward flow into a jet, bringing relatively saline water from the tropical eastern Pacific to the entire subarctic continental slope [*Thomson and Krassovski*, 2010]. The change in sign of the offshore gradient above the undercurrent indicates the transition to coastal upwelling. Below the near-surface waters, we observe weak long-term warming above the core of the undercurrent, likely reflecting opposing temperature

tendencies at a given depth from climate change and an observed dynamical shoaling of constant potential density surfaces [*Meinvielle and Johnson*, 2013].

The magnitude and statistical significance of the warming trend increase with depth below the undercurrent, reaching a maximum between 300 and 600 m depth (Figure 2c) at a rate that is comparable to the global average temperature trend at similar depth and latitude [*Rhein et al*., 2013]. The percentage of equatorial source water over the continental slope declines below the undercurrent core to less than 30% by 500 m depth off Oregon [*Thomson and Krassovski*, 2010]. In 2013, water at 300–600 m depth sampled at the upper continental slope had potential density (σ_θ) between 26.78 and 27.09 kg m^{-3}, averaging 26.97 σ_θ at 480 m. (Note that in the absence of any salinity change, the estimated warming of 0.29°C at this depth would have lowered the potential density by 0.04 kg m^{-3}.) The primary water mass in this density range is North Pacific Intermediate Water (NPIW), with a characteristic low-salinity end-member established in the far western Sea of Okhotsk [*Reid*, 1965; *Talley*, 1993]. NPIW is traditionally defined only within the subtropical gyre, where it is associated with a characteristic salinity minimum. However, after crossing the Pacific, a fraction of the water in the NPIW density range turns northward following the counterclockwise subarctic gyre. At Ocean Station P (50°N, 145°W), western subarctic gyre water contributes over 50% of the water mass mixture at 26.7 σ_θ [*Whitney et al*., 2007].

The transit time via ocean currents from the open-ocean western to eastern Pacific subarctic gyre is approximately one to two decades for 26.7 to 27.2 σ_θ [*Ueno and Yasuda*, 2003]. Temperature changes can also occur via isotherm shifts associated with geostrophic adjustment of ocean circulation to atmospheric forcing, particularly on the margin, where coastal waves can efficiently transmit circulation changes. On the Washington margin, deepening isopycnals below the core of the California Undercurrent suggest that the warming we observe may, in part, reflect the geostrophic signature of increasing transport in the undercurrent [*Meinvielle and Johnson*, 2013]. A change in the mixing ratio between Sea of Okhostk water and Oyashio Current water could also result in a temperature trend in the NPIW [*Kouketsu et al*., 2010]. However, over the long term, sea surface warming in water mass formation regions will be communicated throughout the remote ocean interior. Recent studies show that since the 1950s, Sea of Okhotsk water in the NPIW density range has warmed at rates higher than we observe off the Washington margin [*Itoh*, 2007; *Nakanowatari et al*., 2007]. A recent study [*Johnstone and Mantua*, 2014] finds that the sea-surface warming along the eastern rim of the subarctic gyre over the last century is correlated to an atmospheric sea level pressure trend, with a leading mode that resembles the PDO spatial pattern. However, the effects of atmospheric dynamical forcing decline rapidly with depth, consistent with the decline of PDO-correlated variability in Figure 2c. Furthermore, the atmospheric pressure trend would be expected to be associated with cooling in the western Pacific [e.g., *Mantua et al*., 1997]. Warming over several decades has also been observed at locations spanning the subarctic Pacific in the NPIW density range [*Whitney et al*., 2007; *Kouketsu et al*., 2010; *Nakanowatari et al*., 2007]. At Ocean Station P, warming on both depth levels and potential density surfaces is evident, with maximum values of just over +0.01°C yr^{-1} at 26.7 to 26.9 σ_θ and a trend of +0.008°C yr^{-1} at 27.0 σ_θ for the period 1956–2006 [*Whitney et al*., 2007].

4. Impact of Seafloor Warming on the Methane Hydrate Reservoir

Over the 43 years of our simulation, the thermal disturbance generated by warming of water in contact with the seafloor propagates 30 m into the sediment column (Figure 3), causing the base of the gas hydrate stability field to shoal by ~13 m (Figure S3 in the supporting information), with a horizontal downslope retreat of ~1 km. The horizontal distance the gas hydrate stability zone (GHSZ) retreats offshore is proportional to the upper margin slope (Figures S1, S2, and S4 in the supporting information). These estimates do not consider advection of seawater or the latent heat of gas hydrate dissociation. The latent heat of dissociation would act to stabilize gas hydrate, whereas gas ebullition drives seawater circulation that would warm the sediment column further enhancing the rate of gas hydrate dissociation [e.g., *Tryon et al*., 2002; *Solomon et al*., 2008]. Thus, these are conservative first-order estimates based solely on conduction of heat. To estimate the volume and mass of gas hydrate that could dissociate, we assume a 5 m thick sulfate reduction zone in 1970, with gas hydrate occurring only below this depth. Assuming an average porosity of 0.63 in the upper 15 m [*Riedel et al*., 2006], and an average gas hydrate saturation of 5% of the sediment pore space, approximately 129–164 m^3 of gas hydrate per meter of margin could dissociate. Thus, warming along the Washington upper continental slope between 1970 and 2013 has the potential to dissociate 0.12 to 0.15 Gg

Table 1. Model Estimates and Projections[a]

Estimated Area of Gas Hydrate Stability Zone Affected by Warming ($m^2\ m^{-1}$ of margin)			
Transect	1970 to 2013	1970 to 2100 linear	1970 to 2100 high emissions
P1	4063	24,378	65,071
P2	4201	21,125	46,990
P3	5179	30,310	82,889
Estimated Mass of Methane Hydrate Dissociated in Gg/m of Margin[b,c]			
Transect	1970 to 2013	1970 to 2100 linear	1970 to 2100 high emissions
P1	0.116	0.696	1.86
P2	0.12	0.603	1.34
P3	0.148	0.865	2.37

[a]Estimates assume that the upper 5 m of sediment column are initially devoid of gas hydrate as a result of the sulfate reduction zone.
[b]Assumes a porosity of 0.634 in the upper 15 mbsf based on the results from Integrated Ocean Drilling Program Site U1329 offshore Vancouver Island [*Riedel et al*., 2006] and an assumed average gas hydrate saturation of 5% of the pore space.
[c]Calculated from the volume considering a methane hydrate density of 9×10^5 g/m^3.

of gas hydrate per meter assuming a Structure I hydrate density of $9 \times 10^5\ g\ m^{-3}$ (Table 1). We consider these estimates to be only first order since the sulfate-methane transition zone (SMTZ) depends on the background methane flux and could be either thicker or thinner than assumed. Furthermore, the depth of gas hydrate first occurrence depends on pore water methane concentrations being at least equal to methane hydrate solubility. This depth is dependent on the rate of in situ methanogenesis, methane flux from below, sedimentation rate, and compaction [*Davie and Buffett*, 2001] and is often substantially deeper than the SMTZ. The thickness of the SMTZ and the first occurrence of gas hydrate in this region lack field constraints.

Taking the average mass of dissociated gas hydrate per meter of margin based on the three transects, we estimate that the total mass of hydrate potentially annually dissociating along the 253 km length of the Washington sector of the Cascadia margin is ~32.4 Tg. This amount of dissociation implies a release of 4.35 Tg of methane—an average rate of 1×10^{11} g of CH_4 per year, about the same as the amount released into the Gulf of Mexico during the *Deepwater Horizon* oil spill in 2010 (~1.36×10^{11} g [*Reddy et al*., 2012]). This hydrate-derived methane flux is approximately 500 times the background "passive flux" to the SMTZ over the same area, assuming an upward pore fluid advection rate of $2\ mm\ yr^{-1}$ and methane concentrations in equilibrium with methane hydrate below the SMTZ [*Hyndman and Davis*, 1992]. Due to the lack of field constraints along the WA upper continental slope, we cannot estimate the fraction of the methane released due to gas hydrate dissociation that is consumed via anaerobic oxidation of methane in the sediments or the fraction that bypasses this filter and is emitted to the water column. However, from northern Washington to northern Oregon, the presence of bubble plumes at the retreating upslope limit of gas hydrate (470–530 m water depth; Figure S5 in the supporting information) suggests that a portion of the methane released by contemporary warming is emitted to the water column, as observed in the Arctic [*Berndt et al*., 2014; *Westbrook et al*., 2009; *Thatcher et al*., 2013].

5. Projected Gas Hydrate Dissociation Through 2100

Projections of future seafloor warming along the Washington upper continental slope range from +0.88°C (linear extrapolation) to +2.4°C (AR4 high-emission scenario) by the year 2100. This thermal disturbance will propagate an additional 68–75 m into the sediment column (Figures 3c and 3d and Figures S1 and S2 in the supporting information). This continued long-term warming will cause a horizontal downslope retreat of the gas hydrate stability zone that ranges from ~1.2 km (linear extrapolation) to 2.8 km (high emissions) over the same period. Using the same assumptions regarding the thickness of the sulfate reduction zone and the first occurrence of gas hydrate, an average of 0.72 to 1.86 Gg of methane hydrate would dissociate per meter of margin by 2100 (Table 1). Multiplying by the Washington margin length, ~470 Tg of gas hydrate is susceptible to warming-induced dissociation by 2100 in the high-emission scenario. This rate (~$0.5\ Tg\ CH_4\ yr^{-1}$), represents the annualized release of a volume roughly quadruple the amount released during the *Deepwater Horizon* spill and ~11% of the yearly flux of methane into the Black Sea [*Reeburgh*, 2007].

6. Conclusion

The dense historical water column data off the Washington margin strongly constrains our model of the impact of ocean warming on gas hydrate dissociation along its upper continental slope. However, a similar downslope retreat of the gas hydrate reservoir likely extends from Northern California to British Columbia and Alaska, following the bifurcating pathway of western subarctic water as it mixes into the boundary current system all along the northeast Pacific margin [e.g., *Reid*, 1965]. The magnitude of warming at the source of NPIW [*Itoh*, 2007; *Nakanowatari et al*., 2007] suggests that the Sea of Okhotsk hydrate reservoir is also affected. The environmental consequences of warming-induced hydrate dissociation along the Cascadia margin may be similar to recent models for the Arctic Ocean that show hydrate dissociation from contemporary bottom water warming playing a role in controlling seawater dissolved oxygen and pH in the coming decades [*Biastoch et al*., 2011]. Our results expand the portion of the gas hydrate reservoir susceptible to contemporary warming to lower latitude deposits and suggest that a larger fraction of gas hydrate could dissociate along continental margins worldwide than previously recognized.

Acknowledgments

S.L.H. and E.A.S. equally contributed to this interdisciplinary project. Support was provided by Department of Energy award DE-FE0013998 to E.A.S. and H.P.J., NSF award 1339635 to H.P.J. and E.A.S., and NSF award 1249552 to R.N.H. S.L.H.'s work was made possible by a sabbatical leave from the University of Washington. We thank Brendan Philip for his assistance in processing the multibeam sonar data. Marie Salmi provided valuable assistance with the figures.

The Editor thanks two anonymous reviewers for their assistance in evaluating this paper.

References

Becker, J. J., et al. (2009), Global bathymetry and elevation data at 30 arc second resolution: SRTM30 PLUS, *Mar. Geod.*, *32*, 355–371.

Berndt, C., et al. (2014), Temporal constraints on hydrate-controlled methane seepage off Svalbard, *Science*, *343*, 284–287.

Biastoch, A., et al. (2011), Rising Arctic Ocean temperatures cause gas hydrate destabilization and ocean acidification, *Geophys. Res. Lett.*, *38*, L08602, doi:10.1029/2011GL047222.

Booth-Rea, G., D. Klaeschen, I. Grevemeyer, and T. Reston (2008), Heterogeneous deformation in the Cascadia convergent margin and its relation to thermal gradient (Washington, NW USA), *Tectonics*, *27*, TC4005, doi:10.1029/2007TC002209.

Boswell, R., and T. S. Collett (2011), Current perspectives on gas hydrate resources, *Energy Environ. Sci.*, *4*, 1206–1215.

Davie, M. K., and B. A. Buffett (2001), A numerical model for the formation of gas hydrate below the seafloor, *J. Geophys. Res.*, *106*, 497–514, doi:10.1029/2000JB900363.

Hickey, B. M. (1979), The California Current system - Hypotheses and facts, *Prog. Oceanogr.*, *8*, 191–279.

Hyndman, R. D., and E. E. Davis (1992), A mechanism for the formation of methane hydrate and seafloor bottom simulating reflectors by vertical fluid expulsion, *J. Geophys. Res.*, *97*, 7025–7041, doi:10.1029/91JB03061.

Itoh, M. (2007), Warming of intermediate water in the sea of Okhotsk since the 1950s, *J. Oceanogr.*, *63*, 637–641.

Johnstone, J. A., and N. J. Mantua (2014), Atmospheric controls on northeast Pacific temperature variability and change, 1900–2012, *Proc. Natl. Acad. Sci. U.S.A.*, doi:10.1073/pnas.1318371111.

Kennett, J. P., K. G. Cannariato, I. L. Hendy, and R. J. Behl (2003), *Methane Hydrate in Quaternary Climate Change: The Clathrate Gun Hypothesis*, AGU, Washington, D. C.

Kouketsu, S., M. Fukusawa, D. Sasano, Y. Kunamoto, T. Kawano, H. Uchida, and T. Doi (2010), Changes in water properties around North Pacific intermediate water between the 1980s, 1990s and 2000s, *Deep Sea Res., Part II*, *57*, 1177–1187, doi:10.1016/j.dsr2.2009.12.007.

Mantua, N. J., S. R. Hare, Y. Zhang, J. M. Wallace, and R. C. Francis (1997), A Pacific interdecadal climate oscillation with impacts on salmon production, *Bull. Am. Meteorol. Soc.*, *78*, 1069–1079.

McDougall, T. J., and P. M. Barker (2011), Getting started with TEOS-10 and the Gibbs Seawater (GSW) Oceanographic Toolbox, SCOR/IAPSO WG127, 28 pp.

Meehl, G. A., et al. (2007), Global climate projections, in *Climate Change 2007: The Physical Science Basis. Contribution of Working Group I to the Fourth Assessment Report of the Intergovernmental Panel on Climate Change*, edited by S. Solomon et al., Cambridge Univ. Press, Cambridge, U. K., and New York.

Meinvielle, M., and G. C. Johnson (2013), Decadal water-property trends in the California Undercurrent, with implications for ocean acidification, *J. Geophys. Res. Oceans*, *118*, 6687–6703, doi:10.1002/2013JC009299.

Nakanowatari, T., K. I. Ohshima, and M. Wakatsuchi (2007), Warming and oxygen decrease of intermediate water in the northwestern North Pacific, originating from the Sea of Okhotsk, 1955–2004, *Geophys. Res. Lett.*, *34*, L04602, doi:10.1029/2006GL028243.

Phrampus, B. J., and M. J. Hornbach (2012), Recent changes to the Gulf Stream causing widespread gas hydrate destabilization, *Nature*, *490*, 527–530.

Reagan, M. T., G. J. Moridis, S. M. Elliott, and M. Maltrud (2011), Contribution of oceanic gas hydrate dissociation to the formation of Arctic Ocean methane plumes, *J. Geophys. Res.*, *116*, C09014, doi:10.1029/2011JC007189.

Reddy, C. M., et al. (2012), Composition and fate of gas and oil released to the water column during the *Deepwater Horizon* oil spill, *Proc. Natl. Acad. Sci. U.S.A.*, *109*, 20,229–20,234.

Reeburgh, W. S. (2007), Oceanic methane biogeochemistry, *Chem. Rev.*, *107*, 486–513.

Reid, J. L., Jr. (1965), Intermediate waters of the Pacific Ocean, in *John Hopkins Oceanographic Studies*, vol. 2, 85 pp., John Hopkins Press, Baltimore, Md.

Revelle, R. R. (1983), Methane hydrates in continental slope sediments and increasing atmospheric carbon dioxide, in *Changing Climate: Report of the Carbon Dioxide Assessment Committee*, pp. 252–261, Natl. Acad. Press, Washington, D. C.

Rhein, M., et al. (2013), Observations: Ocean, in *Climate Change 2013: The Physical Science Basis. Contribution of Working Group I to the Fifth Assessment Report of the Intergovernmental Panel on Climate Change*, edited by T. F. Stocker et al., Cambridge Univ. Press, Cambridge, U. K., and New York.

Riedel, M., T. S. Collett, M. J. Malone, and the Expedition 311 Scientists (2006), *Proceedings of the Integrated Ocean Drilling Program*, Expedition 311, Integrated Ocean Drilling Program Management International, Washington, D. C., doi:10.2204/iodp.proc.311.109.2006.

Ruppel, C. D. (2011), Methane hydrates and contemporary climate change, *Nat. Educ. Knowl.*, *3*, 29.

Sandwell, D. T., and W. H. F. Smith (2009), Global marine gravity from retracked Geosat and ERS-1 altimetry: Ridge segmentation versus spreading rate, *J. Geophys. Res.*, *114*, B01411, doi:10.1029/2008JB006008.

Solomon, E. A., M. Kastner, H. Jannasch, G. Robertson, and Y. Weinstein (2008), Dynamic fluid flow and chemical fluxes associated with a seafloor gas hydrate deposit on the northern Gulf of Mexico slope, *Earth Planet. Sci. Lett.*, *270*, 95–105.

Stocker, T. F., et al. (2013), Technical summary, in *Climate Change 2013: The Physical Science Basis. Contribution of Working Group I to the Fifth Assessment Report of the Intergovernmental Panel on Climate Change*, edited by T. F. Stocker et al., Cambridge Univ. Press, Cambridge, U. K., and New York.

Talley, L. D. (1993), Distribution and formation of North Pacific Intermediate Water, *J. Phys. Oceanogr.*, *23*, 517–537.

Thatcher, K. E., G. K. Westbrook, S. Sarkar, and T. A. Minshull (2013), Methane release from warming-induced hydrate dissociation in the West Svalbard continental margin: Timing, rates, and geologic controls, *J. Geophys. Res. Oceans*, *118*, 22–38, doi:10.1029/2012JB009605.

Thomson, R. E., and M. V. Krassovski (2010), Poleward reach of the California Undercurrent extension, *J. Geophys. Res.*, *115*, C09027, doi:10.1029/2010JC006280.

Tishchenko, P., C. Hensen, K. Wallmann, and C. S. Wong (2005), Calculation of the stability and solubility of methane hydrate in seawater, *Chem. Geol.*, *219*, 37–52, doi:10.1016/j.chemgeo.2005.02.008.

Tryon, M. D., K. M. Brown, and M. E. Torres (2002), Fluid and chemical flux in and out of sediments hosting methane hydrate deposits on Hydrate Ridge, Or, II: Hydrological processes, *Earth Planet. Sci. Lett.*, *201*, 541–557.

Ueno, H., and I. Yasuda (2003), Intermediate water circulation in the North Pacific subarctic and northern subtropical regions, *J. Geophys. Res.*, *108*(C11), 3348, doi:10.1029/2002JC001372.

Wang, K., R. D. Hyndman, and M. Yamano (1995), Thermal regime of the Southwest Japan subduction zone: Effects of age history of the subducting plate, *Tectonophysics*, *248*, 53–69.

Westbrook, G. K., et al. (2009), Escape of methane gas from the seabed along the West Spitsbergen continental margin, *Geophys. Res. Lett.*, *36*, L15608, doi:10.1029/2009GL03191.

Whitney, F. A., H. J. Freeland, and M. Robert (2007), Persistently declining oxygen levels in the interior waters of the eastern subarctic Pacific, *Prog. Oceanogr.*, *75*, 179–199.

Zhang, Y., J. M. Wallace, and D. S. Battisti (1997), ENSO-like interdecadal variability: 1900–93, *J. Clim.*, *10*, 1004–1020.